Design and Optimization of Artificial Reef Materials and Structures for Intelligent Ocean Ranching: A Neural Network and CFD Approach

Qichao Yang[1,†], Liren Zhang[1,*,†], Zhenbo Li[1,†], Junyi Jiang[1], Pengye Jiang[2]

[1] Dalian University of Technology, Dalian, China

[2] Tianjin University, Tianjin, China

[*] Email: 1350232465@qq.com

[†]These authors contributed equally

Abstract

This study focuses on the design and optimization of artificial reef materials and structures for ocean ranching. By incorporating fly ash, a major solid waste, into reef materials, we aim to achieve resource utilization and carbon emission reduction. BP neural network models are used to predict the composition ratio of concrete to meet expected mechanical properties. Two types of reef structures, "deflector - type" and "upwelling - type," are designed and analyzed through fluid dynamics simulations. The "deflector - type" reef is selected based on the results. Additionally, a customized cement 3D printer is developed to fabricate the reefs. Experimental studies on fish behavior responses to the reefs are also conducted. The results provide a theoretical basis and technical support for the construction of intelligent ocean ranches.

Keywords

Artificial reef, fly ash, BP neural network, fluid dynamics, 3D printing, fish behavior.

1. Introduction

Artificial reefs play a crucial role in enhancing the aquatic environment, providing habitats for fish and other marine organisms, and promoting fishery resource conservation and growth. In China, although significant progress has been made in artificial reef construction, there are still challenges in material selection, structural design, and optimization compared to developed countries. With the global emphasis on carbon neutrality and sustainable development, it is essential to find new ways to improve the efficiency of artificial reef construction while reducing environmental impacts.

Fly ash, a large - scale solid waste, can be effectively utilized in artificial reef materials. Incorporating fly ash into concrete used for reefs can improve its physical and mechanical properties, such as strength, durability, and crack resistance, while reducing cement consumption and carbon emissions.

The design of artificial reef structures also needs to be optimized. Traditional reef structures may not fully meet the ecological and functional requirements. By using computational fluid dynamics (CFD) and neural network technologies, we can design more suitable reef structures to enhance their ecological and economic benefits.

2. Literature Review

2.1. Overseas Research on Artificial Reefs

Norway is at the forefront of deep - sea reef research. Researchers like Lars - Petter Granli, Svein Løkkeborg, and Tore Strohmeier have found that deep - sea reefs in Norwegian waters can accommodate over 200 benthic organisms per square meter on average. These reefs provide rich habitats and promote the growth of deep - sea fishery resources, attracting commercial fish species such as cod and flounder (Granli, L. - P., Løkkeborg, S., & Strohmeier, T., [Publication Year]).

The United States has a long history of artificial reef research. In 1935, the first artificial reef in the world was built near Cape May, New Jersey. After World War II, the reef - building scope expanded. In 1968, the US government proposed the Ocean Ranching Plan, and in 1972, the construction of artificial reefs was legally protected. The research by Robert Ballard, Sylvia Earle, and Jane Lubchenco shows that artificial reefs deployed along the US coast have recorded over 400 species of fish and invertebrates, promoting both marine tourism and fishery resource development (Ballard, R., Earle, S., & Lubchenco, J., [Publication Year]).

2.2. Domestic Development of Artificial Reefs

China started fish stock enhancement and marking experiments in the coastal areas of Zhejiang and Jiangsu in the 1930s. In the late 1970s, China began to construct artificial reefs, and in the early 21st century, explored the construction of ocean ranches based on artificial reefs and marine organism enhancement. In 1979, the artificial reef experimental research was carried out in the Beibu Gulf of Guangxi, and then widespread experiments were conducted in coastal provinces such as Guangdong, Liaoning, Shandong, Zhejiang, Fujian, and Guangxi. Since 2006, the Chinese government has clearly regarded artificial reefs and ocean ranches as measures for fishery resource enhancement ([Citation of relevant domestic research], [Publication Year]).

3. Research Methodology

3.1. Research on Seabed Reef Materials

We consider the erosion of seawater on reefs, material strength, and biological adhesion. A BP neural network model is established to predict the composition ratio of concrete. We use the control variable method to make 120 "8" - shaped workpieces with different concrete compositions. Through uniaxial tensile tests, compressive strength tests, and other experiments, 647 rows of experimental data are collected for training the neural network model.

The trained BP neural network model is integrated into software. The input interfaces are set as expected fracture toughness, cracking strength, elastic modulus, compressive strength, and tensile strength. According to the neural network algorithm, the composition ratios of concrete to achieve the expected mechanical properties are calculated.

3.2. Research on Seabed Reef Structures

Two types of external frameworks for reefs, the "deflector - type" and "upwelling - type," are designed. Each framework is placed in a 200×200×200mm fluid domain and analyzed in ANSYS Workbench 2021 under horizontal and 45 - degree water flow impacts.

First, the reef is meshed using the Geometry plugin interface to establish a finite - element model. Then, it is imported into the Fluent interface, where boundary conditions and material parameters are set for analysis. The analysis results include structural surface pressure nephograms, cross - section velocity nephograms, structural stress nephograms, and structural displacement nephograms. Based on these results, the "deflector - type" reef is selected.

For the internal structure design of the reef, considering the natural formation process of reefs by ocean current scouring and coral excrement and carcass deposition, we use the fluid - solid coupling idea in the finite - element analysis software. The external framework is meshed, and a finite - element model is established. The left - hand side has an upper and lower water inlet and sediment inlet, and the right - hand side has a common outlet. The solution basis is set as pressure - based considering gravity. The Eulerian multiphase flow is selected for the analysis model, and the standard k - e turbulence model is used for liquid viscosity. After setting the material - related parameters, calculations are carried out, and output results include blue trajectory diagrams, middle - section sediment - water volume fraction distribution diagrams, deposition process diagrams, and sediment - deposited surface morphology diagrams.

We also use the behavior analysis software LoliTtrack Version 5 to record and analyze the behavior responses of fish schools to the reef external framework. Twenty healthy experimental individuals with no surface damage are selected, and a camera is used to record every 15 minutes for 1 minute each time, for a total of 5 hours. The approximate activity behavior trajectory diagram of the fish school is obtained. The internal structure of the reef is finally determined by integrating the simulation results of reef scouring and deposition and the fish school behavior analysis.

3.3. Research on Cement 3D Printers

Based on the open - source assembly diagrams of cement 3D printers[1] available online, we optimize and design a cement 3D printer suitable for printing seabed reefs. To address the technical challenges of cement 3D printers, such as control of cement setting time, fluidity, extrudability, pumpability, supportability, and low early - age compressive strength, solutions are proposed, including the use of retarders and accelerators, thickeners or fibers, modification of the nozzle internal pipeline layout, installation of drying equipment inside the nozzle, and adjustment of the nozzle movement speed.

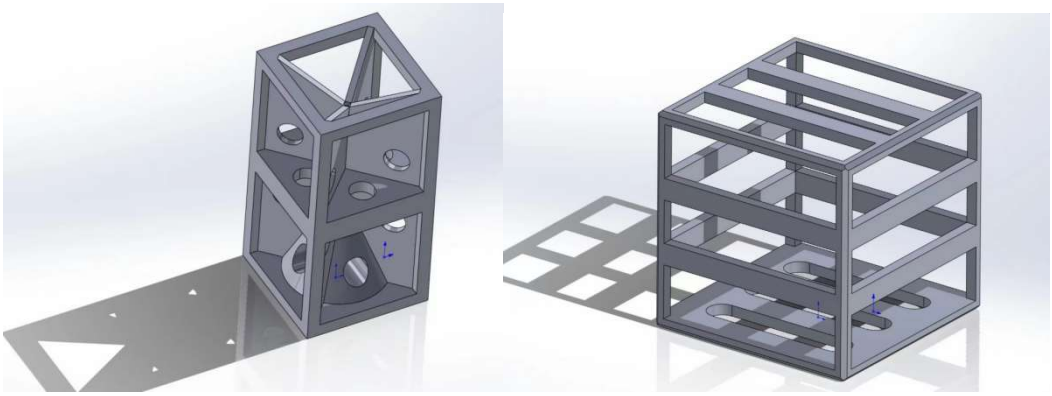

Figure 1. Deflector plate type reef (left) and upwelling type reef (right)

4. Experimental Results and Analysis

4.1. Results of the BP Neural Network Model

The trained BP neural network model[2] can predict the composition ratio of concrete with high accuracy. For example, when the expected mechanical properties are set as a fracture toughness of 0.5 MPa·m^0.5, a cracking strength of 1.8 MPa, an elastic modulus of 8 MPa, a compressive strength of 20 MPa, and a tensile strength of 2.4 MPa, the model predicts the mass percentages of fly ash, oyster shell, and sand in the concrete, providing a scientific basis for the preparation of artificial reef materials.

The overall processing flow of this scheme is shown in Figure 2. The processing procedure is mainly divided into three parts, namely data collection, data preprocessing, and training and optimizing the model[3].

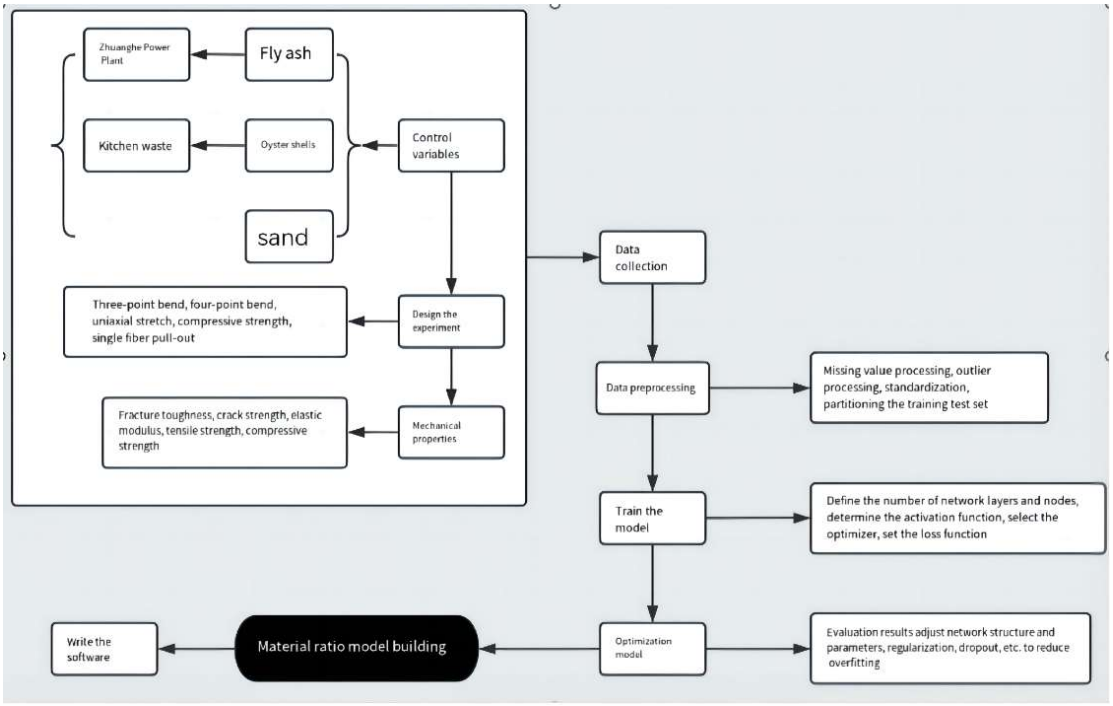

Figure 2. Overall processing flow chart

4.1.1. Data Collection:

First, the control variable method is adopted to change the mass percentages of fly ash, oyster shells, and sand in the experimental specimens. Three - point bending, four - point bending, uniaxial tension, compressive strength, and uniaxial fiber pull - out tests are carried out. The corresponding fracture toughness, cracking strength, elastic modulus, tensile strength, and compressive strength of each group of specimens are obtained. The mass percentages of the components and the mechanical properties of each group of experimental specimens are used as inputs for model training and prediction.

4.1.2. Pre - processing:

After obtaining the experimental data set, the data set is first screened to remove outliers, avoiding the over - fitting problem of the model. Then, different types of feature data are standardized to unify them on the same scale[4]. The pre - processed experimental data set is divided into a training set and a test set. The training set is used for model training. After the training is completed, the test set is used to test the model performance. Then, data standardization is carried out. The mass percentages of components and the characteristic values of various mechanical properties have different dimensions and large numerical differences. Directly inputting them into the model will affect the training results and reduce the training speed. To accelerate the training convergence, the data set needs to be normalized in the experiment. Use the maximum value x_{max} and the minimum value x_{min} in the data to map all the original data x_{origin} to the interval [0,1]:

$$x_{new} = \frac{x_{origin} - x_{min}}{x_{max} - x_{min}}$$

The gross errors in the data set may make *xmax* too large, resulting in unstable normalization results and further affecting the final prediction effect. Therefore, the gross errors in the data set need to be removed before modeling. Define the data in which only the mass percentage of one component is changed in the above - mentioned control variable method as homologous data. Extract the five mechanical properties of the homologous data and use the standard deviation method to detect outliers. The detected outliers are determined as gross errors, and the entire arc - segment data where the gross errors are located is removed.

4.1.3. Model Training and Optimization:

The input layer of the BP neural network contains 5 nodes, corresponding to 5 mechanical properties respectively; it has 3 hidden layers, with 64 nodes in each layer[5]. The ReLU activation function is used, and regularization techniques (such as dropout) are adopted to reduce the risk of over - fitting; the output layer has 3 nodes, corresponding to the mass percentages of fly ash, oyster shells, and sand. The sigmoid function is used, and the output is multiplied by 100. The mean squared error (MSE) is used as the loss function. The smaller the loss function value is, the closer the predicted value of the model is to the true value *y*, that is, the better the model is. The Adam optimizer is selected, which combines the advantages of RMSprop and momentum gradient descent. The MSE is as shown in the following formula:

$$\mathrm{MSE} = \frac{\mathrm{SSE}}{\mathrm{n}} = \frac{1}{\mathrm{n}}\sum_{\mathrm{i}=1}^{\mathrm{m}} \mathrm{w_i}(\mathrm{y_i} - \hat{\mathrm{y}_\mathrm{i}})^2$$

4.1.4. Desktop Processing of Algorithms:

Based on the above-mentioned trained neural network algorithm, we wrote the program using the Dart language on the Flutter framework to enable it to perform desktop operations on the Windows system. The software is named NeuroReefAnly and its interface is shown in the picture.

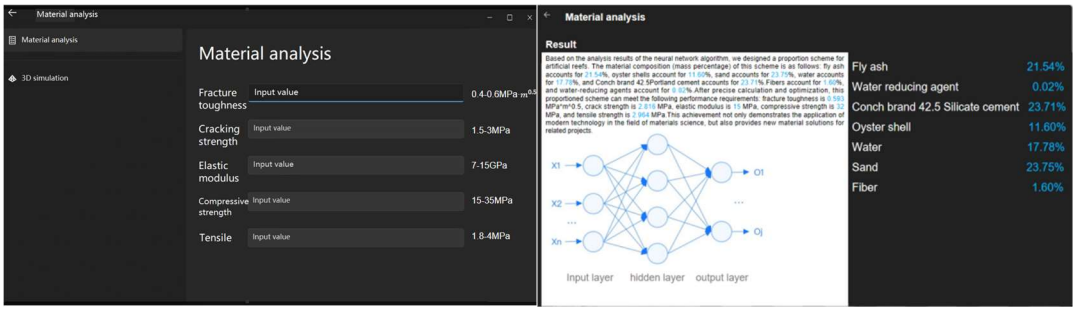

Figure 3. Schematic diagram of the software

The right picture shows the input interface. Users input the valid values and click "Analyze". After model training, the left picture output interface can be obtained. The output interface includes the model summary and the material ratio of the artificial reef.

4.2. Fluid Dynamics Analysis Results

4.2.1. Fluid Analysis:

To study the impact force of the upwelling fish reef on the seabed shown in Figure 1 above, we conducted fluid analysis on the structural stress field distribution and displacement distribution caused by the water flow impact in the underwater environment through fluid-structure coupling analysis, as well as the flow field distribution of the fluid itself.[6]

Let's assume that the structural components are surrounded by water. We respectively establish fluid domains of 200×200×200mm and 200×350×350 to enclose the solid domains,

as shown in Figure 4. The water flow impact in two directions was simulated during the analysis, as shown in Figure 5.

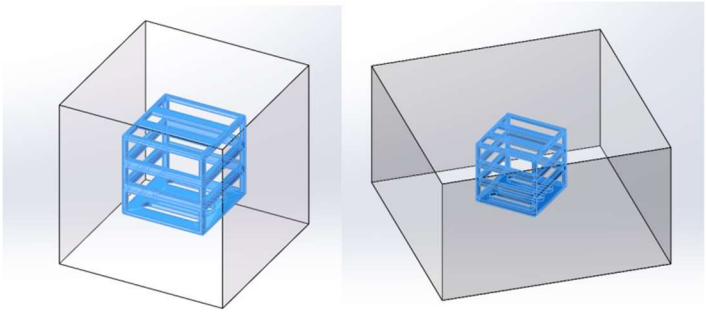

Figure 4. three-dimensional model illustration (the transparent area is the fluid domain)

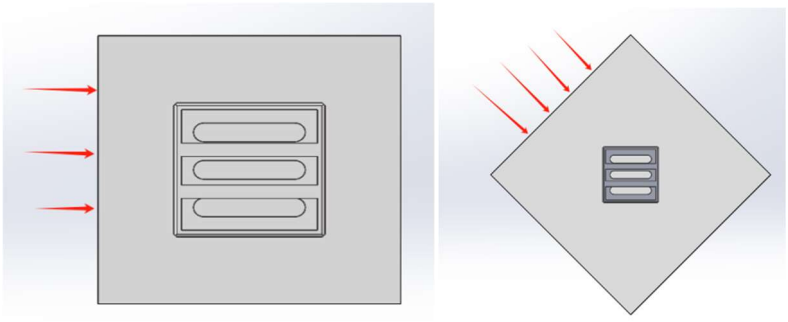

Figure 5. Illustration of flow field scouring angles (horizontal and 45°)

We adopt ANSYS Workbench 2021 as the analysis software and will apply it to the two analysis modules of fluid analysis (Fluent) and Static Structure analysis[7]. The established three-dimensional model was imported into the finite element analysis software through "Geometric Structure" for meshing. The size of the element was controlled at 5mm. The meshing result is shown in Figure 6.

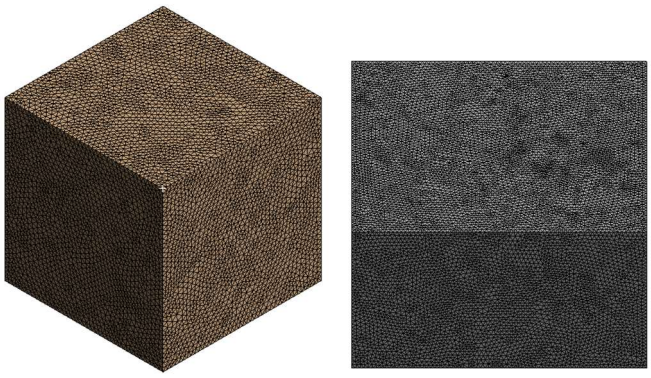

Figure 6. Grid division (horizontal top, 45° bottom)

In Fluent, enter the fluid analysis module, set the solution class as the pressure basis[8], conduct steady-state analysis, and do not consider the effect of gravity. Fluid analysis is based on the analysis and calculation under the law of conservation of energy. Therefore, the energy equation needs to be opened, and then the water flow is assumed to be laminar flow. Add liquid water materials to the material library and assign them to the corresponding solid domains and fluid domains through unit area conditions, and then define the boundaries. Finally, standard

initialization was selected and the number of iterations was set to 100 for solution calculation[9]. After the calculation is completed, the required result images are extracted through post-processing, as shown in the following figure.

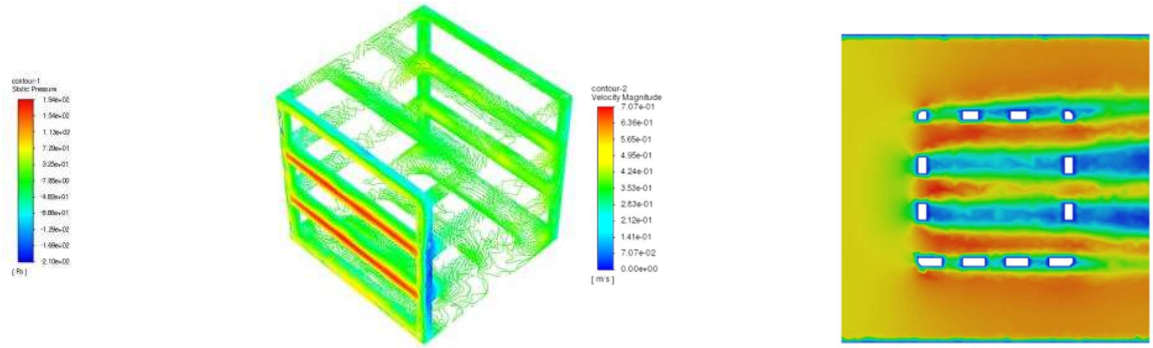

Figure 7. shows the surface pressure cloud map and cross-sectional velocity cloud map of the structural components subjected to horizontal scouring

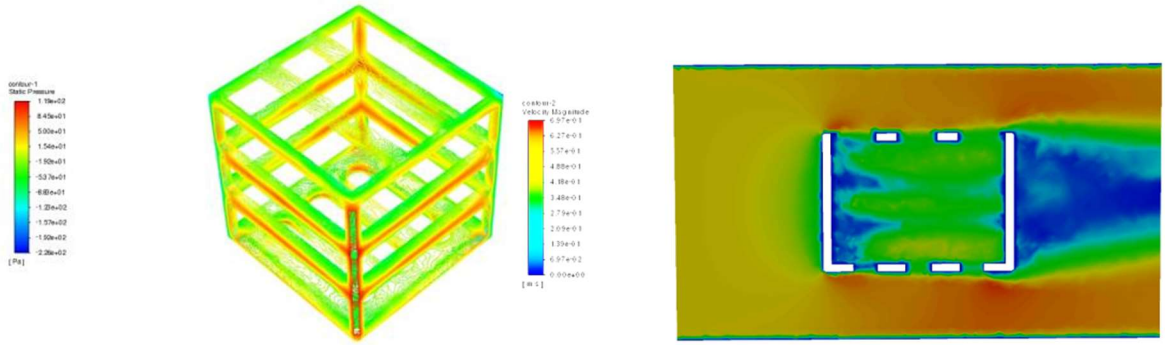

Figure 8. shows the surface pressure cloud map and cross-sectional velocity cloud map of the structural components washed at 45°

4.2.2. Structural statics Analysis:

After the fluid analysis is completed, the pressure acting on the outer surface of the structural components at various locations during the fluid analysis is read through the statics analysis module, and then the structural response is analyzed. Based on one of the representative artificial reef materials, the material parameters are set as shown in Table 1:

Table 1. Material Parameter Table

Materials	Elastic modulus (N/m^2)	Poisonby	Mass density (kg/m^3)	Yield strength (Mpa)
Aluminum alloy	6.90E10	0.330	2.70E3	270Mpa

Then, consistent with the aforementioned grid division, adaptive grid division is adopted to control the overall cell size to 2mm. Fix the bottom surface of the structural components, add fixed supports, and import the pressure on each surface in the fluid analysis through the "Imported load" interface. After the loading is completed, carry out the solution calculation. Finally, the structural stress cloud map and deformation cloud map can be obtained, as shown in the following figure[10].

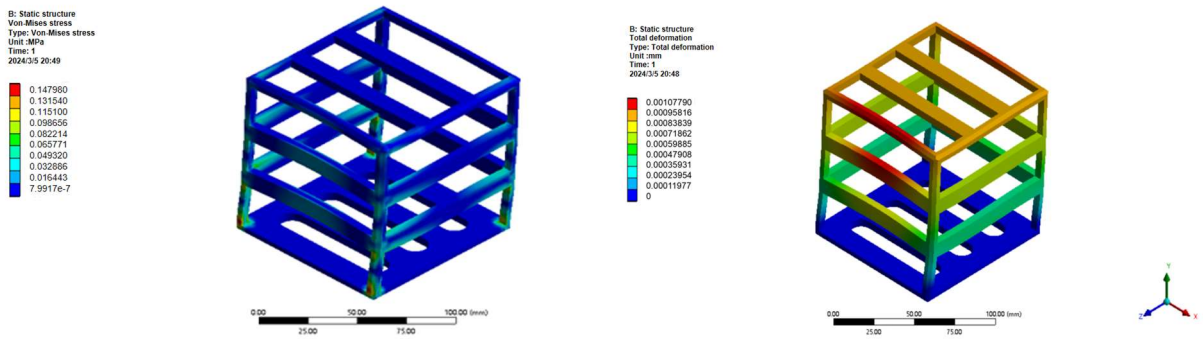

Figure 9. Stress cloud map and displacement cloud map of structural components subjected to horizontal scouring

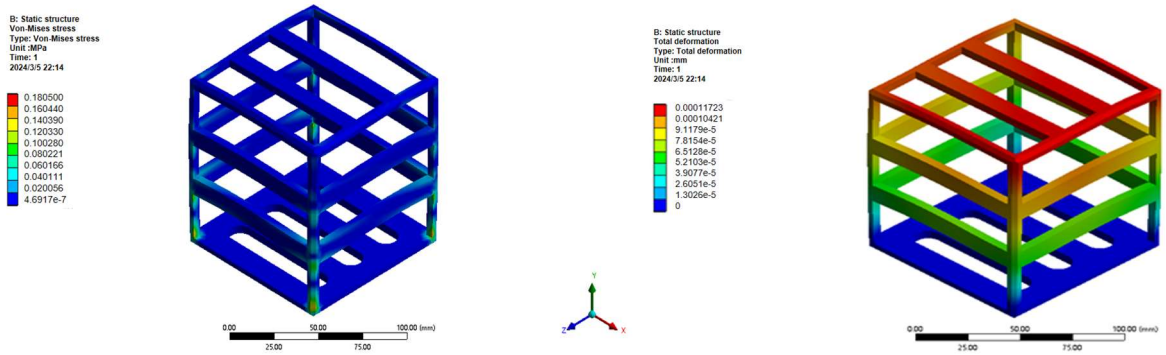

Figure 10. shows the stress cloud map and displacement cloud map of the structural components washed at 45°

The fluid dynamics analysis of the "deflector - type" and "upwelling - type" reefs shows different flow field characteristics. The "deflector - type" reef can better adjust the flow field around the reef, which is conducive to the aggregation of fish and the deposition of nutrients. The pressure and velocity distribution nephograms obtained from the analysis help us understand the hydrodynamic performance of the reefs and provide a reference for structural optimization.

The structural stress and displacement nephograms obtained from the static structural analysis show that the designed reef structures can withstand[11] the impact of water flow. The stress and displacement values are within the allowable range, indicating the structural stability of the reefs.

4.3. 3D Simulation Results of Reef Scouring and Formation

The 3D simulation of reef scouring and formation shows the process of sediment deposition and the final sediment - deposited surface morphology. The results help us understand how the reef interacts with the seabed environment and provide a basis for further improving the reef structure to adapt to the natural environment.

The final output results yield the distribution map of the volume fraction of sediment and water in the middle section, the schematic diagram of the sediment deposition appearance (Figure 11), and the animation of the sediment deposition process (Figure 12).

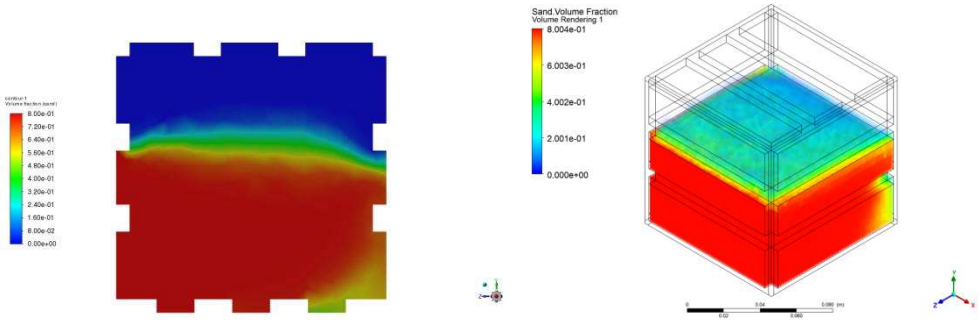

Figure 11. shows the distribution map of the volume fraction of sediment and water in the cross-section and the schematic diagram of the sediment deposition surface

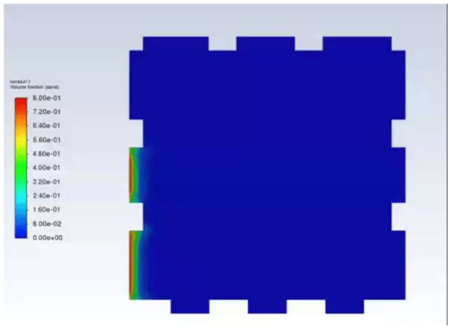

Figure 12. Animation of sediment deposition process

4.4. Fish Behavior Response Experimental Results

The experiment on the behavior responses of fish schools to the artificial reef shows that the introduction of artificial reefs can enhance the reef - seeking behavior of loach fry. Although the fry initially show a tendency to gather in the corners of the tank, after an adaptation period, more and more fry start to explore and stay near the artificial reef. The activity ability of the fry also increases. The activity trajectory probability map of the fish school obtained from the analysis provides a reference for optimizing the internal structure of the reef.

Figure 13. Physical picture of upwelling fish reefs

4.4.1. Experimental Observation Method

An observational experiment was conducted to assess the influence of artificial reefs on fish behavior. A high - resolution digital camera (model: [specify camera model]) was positioned vertically above the experimental water body, directly over the designated area for artificial reef deployment, to ensure unobstructed and comprehensive monitoring.

Two distinct experimental groups were established: a blank control group and an experimental group. In the blank control group, no artificial reef models were placed within the experimental area, serving as a baseline for comparison. Conversely, the experimental group featured the

placement of the pre - fabricated artificial reef model, as described in previous sections, in the designated artificial reef model area.

For each experimental trial, ten healthy fish specimens were carefully selected from the breeding pool. These fish were required to exhibit no visible signs of physical damage on their body surfaces and demonstrate robust vitality, as determined by active swimming behavior and normal physiological responses. Prior to the commencement of each experiment, the selected fish were transferred to a holding water tank and allowed to acclimate to the new environment for 15 minutes. This acclimation period aimed to minimize any potential stress - induced behavioral changes that could confound the experimental results.

Subsequently, the artificial reef model was precisely positioned in the designated location within the experimental water body, and video recording was initiated immediately. The camera was configured to operate in an interval - shooting mode, capturing a 1 - minute video segment every 15 minutes. This recording protocol was maintained for a total duration of 5 hours per experiment, ensuring sufficient data collection to analyze temporal variations in fish behavior.

Behavioral analysis of the recorded videos was performed using LoliTtrack Version 5, a specialized behavioral analysis software developed by Loligo® Systems. Specifically, the movement and distribution patterns of ten fish fry were meticulously analyzed. To enhance the reliability and validity of the experimental results, each experimental trial was replicated multiple times, and the data obtained from all replicates were aggregated for comprehensive statistical analysis. A detailed flowchart illustrating the entire experimental process is presented in Figure 14, providing a visual representation of the experimental design and procedures.

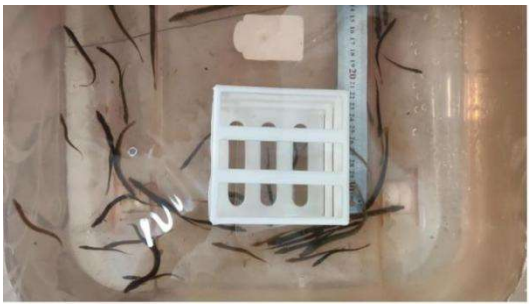

Figure 14. Experimental process record diagram

4.4.2. Experimental Analysis and Findings

In the course of this experiment, no significant rejection behavior of the experimental fish fry towards the artificial reef model was observed. The data from the control group, where no artificial reefs were present, revealed that the fish fry displayed low spatial stability within the experimental water tank. Specifically, they predominantly aggregated at the four corners of the tank, likely due to seeking shelter and perceiving these areas as safer zones without any structural features.

Conversely, in the experimental group, upon the introduction of artificial reefs, an interesting behavioral transition was noted. Initially, the fish fry showed little inclination to approach the reef structures, continuing to cluster in the tank corners and avoid the reef - occupied regions. This initial avoidance may be attributed to the novelty of the reefs, which introduced an unfamiliar environmental element that triggered a cautious response in the fish fry. However, following an adaptation period, a small number of fish fry began to explore the artificial reefs, venturing into their internal cavities. Nevertheless, their sojourn time within the reefs remained relatively brief, indicating a degree of hesitancy or wariness.

As the experimental duration extended, a notable shift occurred, with the majority of fish fry gradually showing a preference for the area surrounding the artificial reefs. This behavioral change suggests that over time, the fish fry recognized the reefs as potential habitats or sources of shelter, overcoming their initial apprehension.

Subsequently, based on the comprehensive analysis of the fish fry's distribution positions and movement capabilities, probability graphs depicting the fish's activity trajectories were generated.

By identifying the routes characterized by the highest density of probability points, valuable insights were obtained for optimizing the internal structure of the artificial reefs. These high - probability routes indicated the preferred movement paths of the fish fry, which could guide the design of more fish - friendly reef architectures. The user interface of the analysis software employed in this process is illustrated in [insert relevant figure number], providing a visual representation of the analytical tools and data visualization techniques utilized.[12]

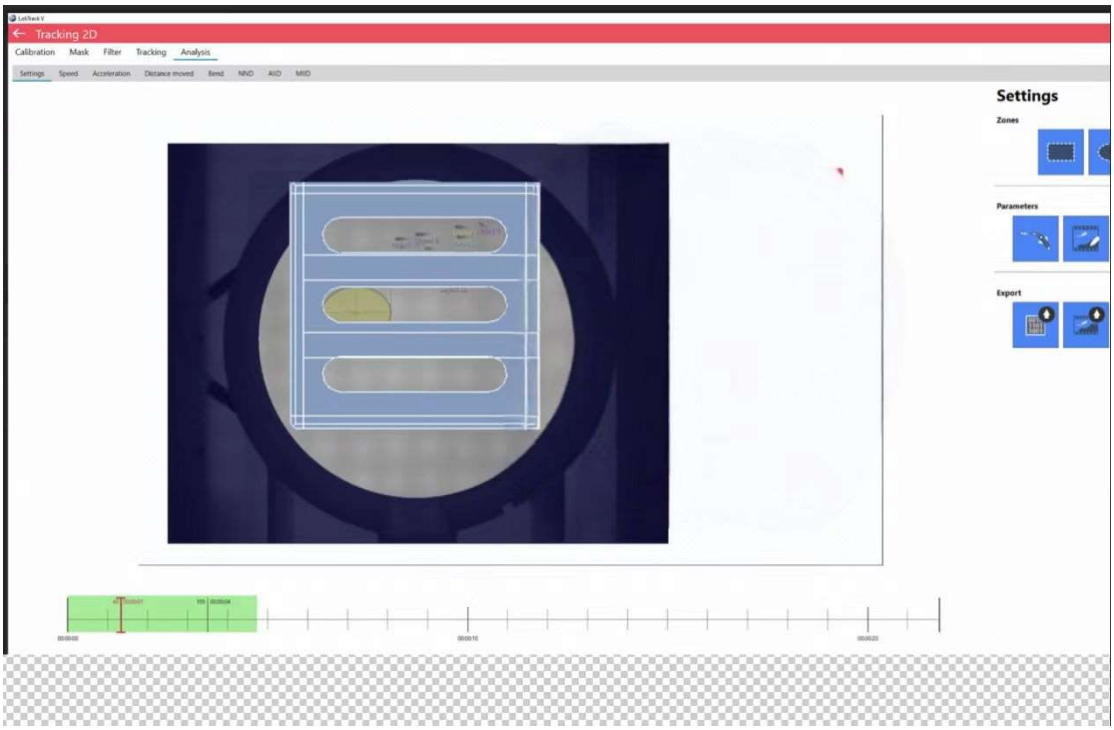

Figure 15. Analyzes the software interface

5. Conclusion

In this study, we have achieved the following results:

A BP neural network model is successfully established to predict the composition ratio of artificial reef materials, which can meet the expected mechanical properties and contribute to the rational use of materials.

Through fluid dynamics simulations, the "deflector - type" reef is selected as the optimal external framework, and the internal structure of the reef is optimized based on the simulation of reef scouring and deposition and fish behavior analysis.

A customized cement 3D printer is developed to fabricate artificial reefs, which provides a new method for reef construction.

The experimental study on fish behavior responses to artificial reefs verifies the positive role of artificial reefs in enhancing fish reef - seeking behavior and activity ability.

However, there are still some limitations in this study. The experimental results are mainly based on loach fry, and the generalization of the conclusions needs to be further studied with different fish species and growth stages. In the future, more in - depth research can be carried out in these aspects to improve the design and application of artificial reefs.

References

[1] Huang, Zicong. “Application of 3D Printing Technology in Marine Fishery Research.” *Open Journal of Fisheries Research*, vol. 6, no. 2, 2019, pp. 73–81. https://doi.org/10.12677/ojfr.2019.62009. Accessed 12 Mar. 2024.

[2] Hager, Izabela, Anna Golonka, Roman Putanowicz, et al. “3D Printing of Buildings and Building Components as the Future of Sustainable Construction?” *Procedia Engineering*, vol. 151, 2016, pp. 292–299. https://doi.org/10.1016/j.proeng.2016.07.357. Accessed 12 Mar. 2024.

[3] Jia, Hang. “Application and Development of 3D Printing in the Field of Architecture.” *Hans Journal of Civil Engineering*, vol. 12, no. 5, 2023, pp. 604–610. https://doi.org/10.12677/hjce.2023.125067. Accessed 12 Mar. 2024.

[4] Li, Chunlin. “Practice and Exploration of Aquatic Science Teaching Based on 3D Printing Technology.” *Advances in Education*, vol. 12, no. 3, 2022, pp. 684–693. https://doi.org/10.12677/ae.2022.123111. Accessed 12 Mar. 2024.

[5] Masuda, Hisaya, Toshiyuki Kusunose, and Takashi Goto. “Additive Manufacturing of SiC Ceramics with Complicated Shapes Using the FDM Type 3D-Printer.” *Journal of Materials Science and Chemical Engineering*, vol. 7, no. 2, 2019, pp. 1–12. https://doi.org/10.4236/msce.2019.72001. Accessed 12 Mar. 2024.

[6] Tan, Kang. “Predicting Compressive Strength of Recycled Concrete for Construction 3D Printing Based on Statistical Analysis of Various Neural Networks.” *Journal of Building Construction and Planning Research*, vol. 6, no. 2, 2018, pp. 71–89. https://doi.org/10.4236/jbcpr.2018.62005. Accessed 12 Mar. 2024.

[7] Zuo, Zibo, Xiangyu Wang, and Yifan Chen. “Performance of 3D Printing in Construction by Using Computer Control Technology.” In *Proceedings of the CENet2017 Conference*, 2017, p. 48.

[8] Zuo, Zibo. “Research and Application of Digital Construction Technology Based on 3D Printing.” *Hans Journal of Civil Engineering*, vol. 7, no. 6, 2018, pp. 765–773. https://doi.org/10.12677/hjce.2018.76092. Accessed 12 Mar. 2024.

[9] Jiang, Manju, Guo Yu, Qin Chuangxin, Pan Wanngni, Yu Gang, and Ma Zhenhua. Behavioral responses of juvenile yellowfin snapper to artificial reef models with different opening shapes and diameters [J/OL]. * Chinese Journal of Fishery Sciences *, 2023.

[10] Chen, Zhigao, Zihao Wu, Ya Ban, et al. Flow Prediction of Tidal River Section Based on Harmonic Analysis and VMD-BP Neural Network [J]. * Journal of Wuhan University (Information Science Edition)*, 2023, 48(8): 1389-1397.

[11] Cai, Zhenrong. Research on Displacement Calculation Method of Elastic Mechanics Based on Neural Network [J]. * Science and Technology Innovation *, 2024, (6): 104-107.

[12] Tang, Yu, Wei Zhang, Xingxing Li, et al. Leo satellite precision orbit prediction based on machine learning [J/OL]. * journal of Wuhan university (information science) *, 2023, 1-17. https://doi.org/10.13203/j.whugis20230411. Accessed 13 Mar., 2024.